

# Aluminum Oxide-Silver Nanoparticle Interfaces for Memristive Applications

Bindu Sharma, M. K. Rabinal\*

(Department of Physics, Karnatak University Dharwad-580003, Karnatak, India)

---

**Abstract:** In the present work, a facile approach to construct a nonvolatile resistive random access memory device based on the heterojunction of silver nanoparticles and aluminum oxide is reported. The device structure consisting of Aluminum-Aluminum oxide-Silver Nanoparticles-Aluminum is used to study the charge transport. The current-voltage measurements of this device clearly show the transition from one state to other in two different steps. Initially, a major transition with the resistance ratio as high as  $10^5$  is obtained for the device whereas the minor transition has resulted one order difference in between its low conducting state and high conducting state. The prepared memristor is found to operate at low operational voltages with better uniformity.

**Keywords:** Charge transport, Nonvolatile resistive memristor, Silver nanoparticles heterojunction with aluminum oxide, SEM and XRD.

---

## I. Introduction

The resistive random access memory (ReRAM) devices based on transition metal oxides have been studied since from 1962 [1], these are two terminal structures that take a transition from low conducting state (off) to high conducting state (on) at a well defined critical voltage. A great attention has been revived towards this field only after the first practical ReRAM device based on titanium oxide [2]. Since then a variety of oxides including simple binary oxide to complex oxides has been investigated exhibiting unipolar/bi-polar non-volatile resistive switching [3-9]. Today, the field has gained a tremendous importance both in the research as well as in semiconductor industries due to its interesting properties such as simple structure, small size, low power consumption, high write/erase speed, good endurance and high scalability [10, 11]. It has been predicted that the phenomenon might manifest well at nano-meter length scale therefore, a great attention has been paid to utilize various nanoparticles of metals, metal oxides and semiconductors in their different morphological forms to constitute these devices.

The various forms of nanomaterials utilized for this purpose are nanowires, quantum dots, nanocrystal, nanocubes, nanodots, nanoislands, and nanorods etc. [9, 12-18]. Attractive performance parameters such as fast switching speed ( $\sim 5$  ns), excellent scalability ( $<10$  nm cell size), long endurance ( $>10^{12}$  cycles), and stable data retention ( $>10$  years) has been reported in case of nanomaterials, exhibiting better compatibility with the complementary metal-oxide semiconductor (CMOS) technology [13, 15,]. Hence, the nanotechnology has not only empowered to reduce the particle size but it has also provided a platform for exploring its potential as a strong competitor towards current Flash memory devices [19, 20]. Thus, taking advantage of this field towards ReRAM device fabrication is highly desirable for future electronics. Despite of a better advancement of the field in terms of its performance parameters, the field is still hampered due to lack of understanding in terms of switching and conduction mechanisms in nanoscale vicinity that control the electrical switching [14, 16].

In this communication, we report a ReRAM device based on the silver nanoparticle (AgNPs) and aluminum oxide ( $\text{Al}_2\text{O}_3$ ) heterojunctions, prepared by simple chemical routes for resistive switching application. Basically, the device has shown non volatile resistive switching whereby the transition from one state to other is achieved in two different steps (major and minor). In case of major transition, the resistive ratio is observed as high as  $10^5$  whereas it is only  $\sim 10^1$  for minor transition case.

## II. Experimental Methods

### 2.1 Materials

All commercially available reagents and anhydrous solvents were used without further purification. Ammonium fluoride (anhydrous), sodium borohydride ( $\text{NaBH}_4$ ) (AR) and acetone (AR) were purchased from sd-fine chemicals, India. Silver nitrate ( $\text{AgNO}_3$ ) and high purity aluminum wire (for evaporation of top metal contact) were taken from Sigma Aldrich. Aluminum plate of thickness 1 mm was purchased from local source. All reactions were carried out under open air. Prior to use, aluminum plate was well cleaned and rinsed with triple distilled water.

### 2.2 Formation of Aluminum Oxide Thin Film

In the present work, thin film of aluminum oxide was grown on a conducting aluminum substrate by a

dip chemical coating method. The formation of thin layer was carried out in an aqueous solution of 500 mM ammonium fluoride at room temperature. Complete dissolution of ammonium fluoride was attained by sonicating in ultrasonication bath. The film was grown by dipping vertically a well cleaned aluminum substrate having dimension (length = 4 cm, breadth = 2 cm and thickness = 0.1 cm) in 6 ml of prepared solution taken in 10 ml beaker. The oxidative reaction between the solution and substrate was confirmed from the bubble formation originated at the surface of substrate and it was allowed for a maximum time of 8 minutes. After the completion of process, substrate was taken out from the solution bath, rinsed well with distilled water and then dried under table lamp. A thin layer of oxide film was clearly observed on the substrate which was then utilized for the construction of nonvolatile memory device.

### 2.3 Synthesis of Silver Nanoparticles

The nanoparticles of silver were prepared by a well known chemical method of sodium borohydride reduction. In a typical synthesis, 1 mM aqueous solution of silver nitrate was prepared in 10 ml solution. In a separate beaker, 25 mM sodium borohydride was prepared in 5 ml distilled water. Both these solutions were well sonicated for few minutes for complete dissolution of precursors. Now, 50  $\mu$ l of sodium borohydride was added to silver nitrate solution along with the continuous stirring. With the addition of sodium borohydride, the transparent solution of silver nitrate started turning to light orange colour which was confirming the temporal evolution of nanoparticles formation. This was repeatedly washed to purify the colloidal solution. These nanoparticles were found stable for many days and were utilized in the same form to construct heterojunction with aluminum oxide film to fabricate ReRAM device.

### 2.4 Device Fabrication and Measurements

The aluminum oxide film grown on aluminum substrate was used for ReRAM device fabrication. Heterojunction of aluminum oxide with silver nanoparticles (AgNPs) was formed by drop casting its thin layer with 200  $\mu$ l of prepared AgNPs solution in open air. This solution was spread on the entire region of grown aluminum oxide film (length = 1.8 cm, breadth = 2 cm) which resulted into 250 nm thick film. Above this layer, aluminum contacts with an area of 1 mm<sup>2</sup> were formed by evaporating pure aluminum using metal evaporator under a shadow mask at a high pressure of 10<sup>-4</sup> torr. With this the device constituted metal- metal oxide- AgNPs -metal heterostructure. The resistive switching behavior of this device was studied by utilizing evaporated Al contact as top electrode whereas the Al substrate as bottom electrode. The electrical contacts to these electrodes were made through two thin tungsten probes with diameter 0.7 mm of conductivity setup which were further connected to BNC connectors by using Keithley 2636 A source meter. All the charge transport measurements were carried out in cyclic voltage sweep mode with biased sweeping voltage applied to the evaporated Al electrode positive and bottom contact as negative, the voltage was zero to positive, positive to zero, zero to negative and negative to zero sequence. A schematic cross-section of our Al/Aluminum oxide-AgNPs/Al prototypes is shown in fig. 1.

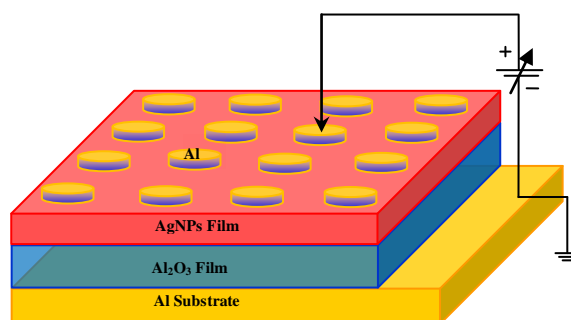


**Fig. 1:** Typical schematic cross-sectional view of Al/Al<sub>2</sub>O<sub>3</sub>-AgNPs/Al resistive random access memory device.

### 2.5 Characterization

The formation of AgNPs was confirmed from XRD, optical absorption and scanning electron microscopic (SEM) measurements, whereas, aluminum oxide film was studied under SEM instrument for morphological growth and elemental analysis. The morphological and elemental analysis was performed using Ultra 55, field emission scanning electron microscope (Carl Zeiss), with EDAX instrument. X-ray diffraction pattern was recorded with Philips X'pert powder diffractometer with Cu  $k_{\alpha 1}$  radiation ( $k_{\alpha 1} = 1.54056 \text{ \AA}$ ). The sample subjected to XRD analysis was prepared by depositing and drying thick film of silver nanoparticles on glass slide. Optical absorption analysis was done using Analytikjena sepcord 200 plus spectrophotometer in the wavelength range 190 – 1100 nm.

### III. Results And Discussion

In order to observe the growth and morphological behavior of aluminum oxide film grown on conducting aluminum substrate, scanning electron microscopy was performed. The obtained results are provided in fig. 2 (a) and (b) for two different resolutions. The lower resolution image of fig. 2(a) confirms the oxidative growth of aluminum oxide on conductive aluminum substrate whereas fig. 2(b) represents higher resolution image consisting of spherically shaped nanoparticles. This confirms that aluminum oxide film has grown in terms of spherical shaped particles with an average size of nearly 40 nm. Since a dense growth of the oxide film can be clearly seen in these micrographs therefore here, we stress that the measured size is an only estimation and to get the exact size high resolution transmission electron microscopy (HRTEM) is must but in the present case, it is out of our scope. Further, the elemental analysis of this film was also carried out to study chemical composition. Carbon tape on metal stub was used as a substrate. Image was scanned at three different places of the sample with a magnification of 2  $\mu\text{m}$ . The EDS analysis of these films confirms that it is stoichiometric in nature that is  $\text{Al}_2\text{O}_3$ .

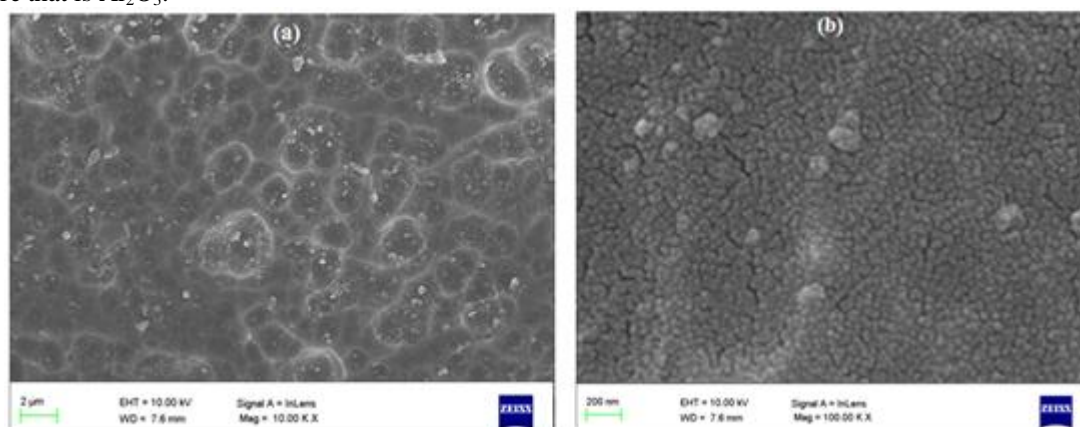


**Fig. 2:** Scanning electron micrographic (SEM) images of aluminum oxide film grown on conducting aluminum substrate (a) at low resolution and (b) at high resolution.

Powder X-ray diffraction studies were employed to access the crystallinity of synthesized silver nanoparticles and the obtained behavior is shown in fig. 3(a). The pattern was recorded in the range  $2\theta = 10^\circ$  to  $90^\circ$  whereas it is given for  $30^\circ$  to  $90^\circ$  in the spectrum. The resultant diffraction pattern clearly shows five well resolved diffraction peaks corresponding to (111), (200), (220), (311) and (222) diffraction planes of silver nanoparticles. The obtained peak values are at  $2\theta = 38.13^\circ, 44.25^\circ, 64.63^\circ, 77.60^\circ$  and  $81.62^\circ$ , these are attributed to FCC crystalline structure of silver. These values are highly consistent with the Joint Committee on Powder Diffraction Standards (JCPDS 04-0784) and are confirmed from reported results [21]. Further, all the peaks confirm that the as synthesized nanoparticles are crystalline in nature. The crystalline size of these is estimated to be  $42 \text{ nm} \pm 0.8$  from (111) diffraction peak using Debye Scherrer formula,  $d = k\lambda / (\beta \cos(\theta))$ ; where  $k$  is Scherrer's constant taken as 0.9,  $\lambda$  is wavelength of radiation,  $\beta$  is full width half maxima and  $\theta$  is Bragg angle. This result is further confirmed from scanning electron microscopic measurements. The micrographic image shown in fig. 3(b) clearly shows that silver nanoparticles are spherical in nature.

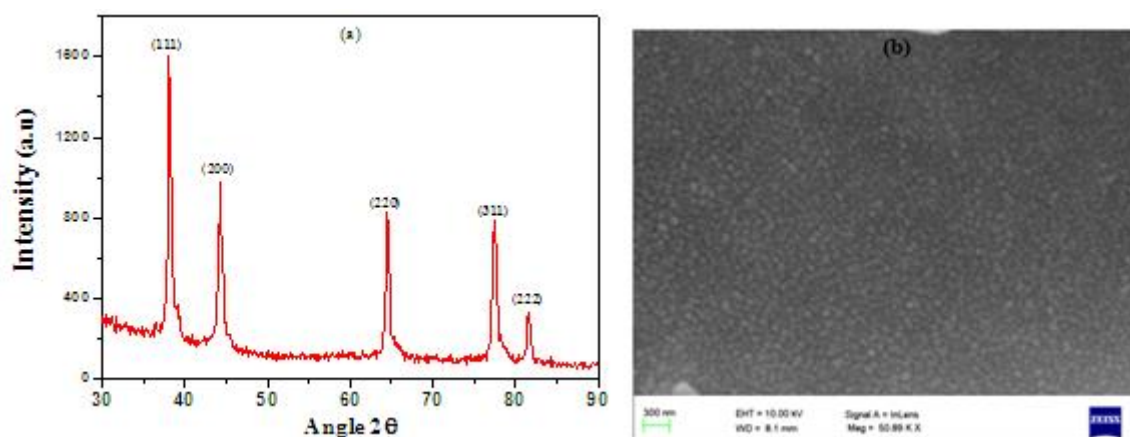


**Fig. 3:** (a) X-ray diffraction spectrum and (b) Scanning electron micrographic image of silver nanoparticles.

The particle size was estimated by taking average of nearly 30 different sized nanoparticles and is calculated as  $\sim 51$  nm which is in good agreement with the estimated size from XRD analysis. The increase in particle size in case of microscopic analysis in comparison with XRD is an obvious result as Debye-Scherrer formula provides the size of the single crystal domain with in which there is periodicity of lattice but the actual nanocrystal always possess wrapping of crystalline domain by disordered non-crystalline layers of its own.

Next, the optical absorption spectrum was recorded for the prepared silver nanoparticles in their colloidal form. The obtained spectrum after normalization is shown in fig. 4. The spectrum clearly shows a sharp surface Plasmon resonance (SPR) peak centered at the wavelength value of 405 nm with a dip at 320 nm, this behavior is typically observed with sodium borohydride reduction in case of silver nanoparticles formation [22, 23]. Further, the peak resonant energy calculated for this SPR peak is 3.07 eV with full width half maximum of only 154 nm.

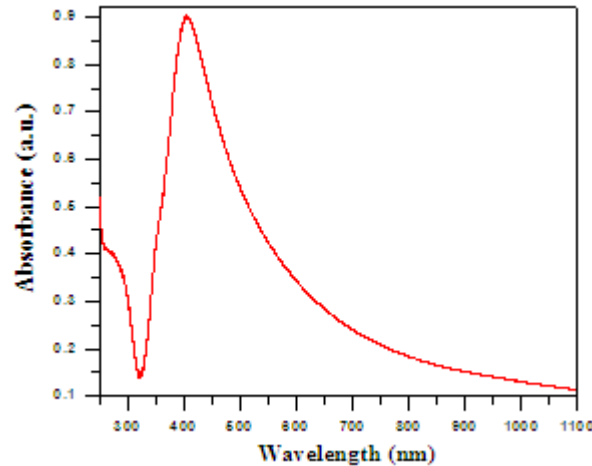


Fig. 4: Optical absorption spectrum of silver nanoparticles recorded in colloidal form.

The charge transport properties of Al/Al<sub>2</sub>O<sub>3</sub>-AgNPs/Al device are shown in fig. 5(a) and 5(b). The measurements were carried out in voltage sweep mode in an ordered sequence of 0 V  $\rightarrow$  +2 V  $\rightarrow$  0 V  $\rightarrow$  -2 V  $\rightarrow$  0 V with a constant scan step of 0.04 V. The resultant I-V curves in fig. 5 (a) are indicating that the device has taken transition to high conducting state in two different steps. The major transition has been taken during first voltage sweep where the device was found initially in a low conducting state (with current  $\sim 10^{-11}$  A), it remained low until a reverse bias with an appropriate voltage of  $-1.87$  V is applied. At this voltage, the device has switched abruptly from low conducting state (with current  $\sim 8.96 \times 10^{-10}$  A) to high conducting state (with current  $\sim 3.85 \times 10^{-5}$  A), these states are known as off and on states of device respectively. The resistance ratio ( $R_{Off}/R_{On}$ ) for these two states is found to be a large nearly equal to  $10^5$ . The second transition which is considerably minor in comparison with the first one was taken by the device when it is scanned after the major transition.

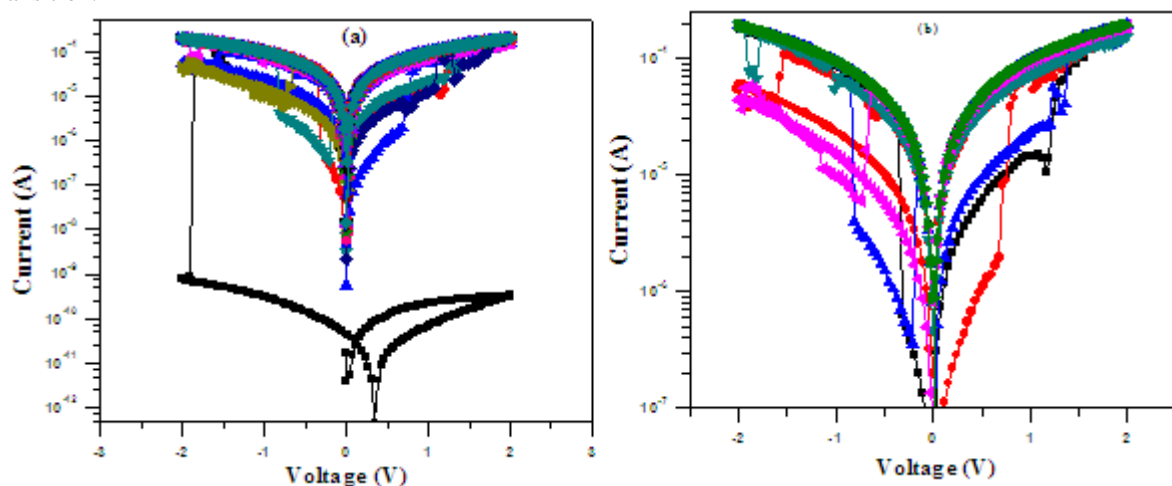
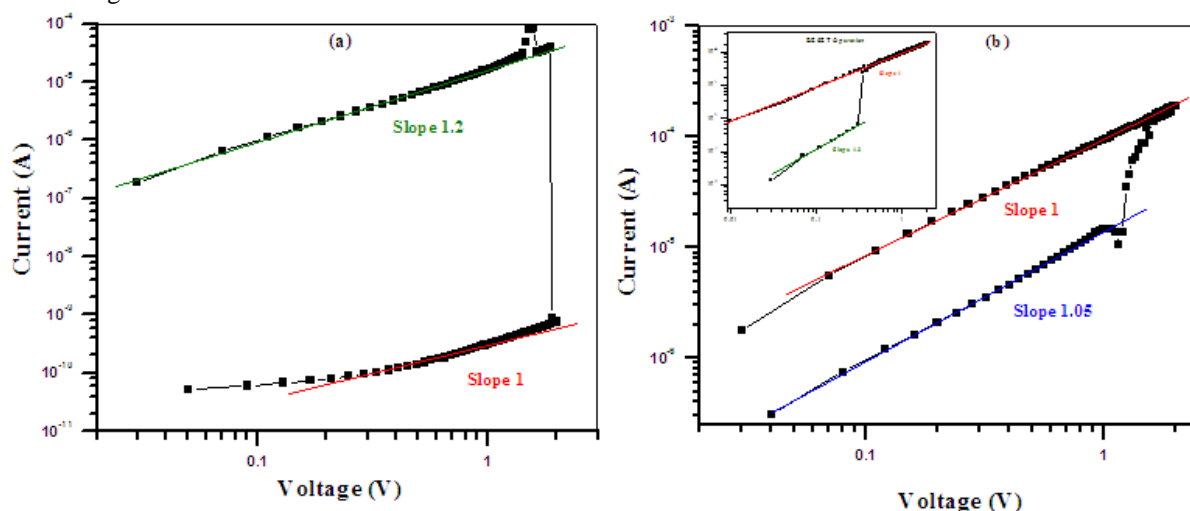


Fig. 5: I-V characteristics of Al/Al<sub>2</sub>O<sub>3</sub>-AgNPs/Al resistive random access memory device (a) semi logarithmic plot, and (b) expanded view of minor transition taken by the device between two more conducting states.

This time the device was switched from the state which was previously set by first voltage sweep to even more high conducting state. For this voltage cycle, the device has shown bipolar resistive switching behavior and the difference between the two states in this case was observed to be nearly of one order in magnitude. With the further repetition of number of voltage sweep cycles, the device was found to be switched alternatively in either of polarities between these conducting states. The expanded view of these behaviors can be seen clearly in fig. 5(b). The repeatability of these measurements can also be seen from the same graph, it is evident that they are quite reproducible.

Next, in order to check the switching mechanism behind this kind of charge transport behavior, the obtained I-V curves were plotted in double logarithmic scale and the obtained results are given in fig. 6(a) and 6 (b). The set process representing the major transition of the device, shown in fig. 6(a) shows that in case of low conducting state, the current response is almost consistent with the ohmic model except slight deviation near low voltage region ( $< 0.28$  V) and threshold region. This is attributed to the thermally generated free electrons at the interface or in the nanoparticles layer from the electron injection. Near to threshold region and after taking the transition, in the high conducting state, device has shown accordance with space charge limited conduction behavior ( $1 < \text{slope} < 2$ ). This behavior shows that the injected electrons from the Al electrode can possibly capture and fill the trapping sites in the oxide film. The electrons are able to flow effectively and continuously through the heterojunction and the current increases sharply around five orders of magnitude as a high conducting state.



**Fig. 6:** Double logarithmic graph representing set/reset operations of the device (a) first set operation, and (b) second set operation. The inset of the fig. 6(b) represents reset operation of the device.

Fig. 6(b) provides the set and reset operations of minor transition taken by the device. From both the graphs it is clear that high conducting and low conducting states during set and reset operations exhibit the same transport mechanisms. For low conducting state, device shows the space charge limited conduction and is almost similar to the high conducting state of major transition. For low conducting state of present case, the device follows the ohm law behavior. Thus as an overall, the device takes transition from ohms behavior to space charge limited current during major transition and then back to ohms law. This kind of transition in two different steps shows that the obtained behavior is a result from the efficient hopping of charge carriers in the film.

#### IV. Conclusions

In summary, we have constructed a resistive random access memory device by utilizing silver and aluminum oxide nanoparticles as memristive elements for charge storage. Simple chemical routes have been employed for nanoparticles synthesis. Dip coating and drop casting techniques were followed for heterojunction formation between the two phases, whereas thermal evaporation technique was employed for creating the top metal contacts. Characteristic nonvolatile resistive switching behavior with low operating voltage was observed for the device. The transition from low to high conducting state was achieved in two different steps. The first step has resulted into major transition with large Off/On ratio of  $10^5$  whereas second transition was observed with one order difference in two conducting states. Here, as our study is focused on a single sized AgNPs, it can also be extended to various other nanoparticles using their different size and morphology. Such studies are crucially important in the design and development of potential memristive devices.

### Acknowledgements

Financial support in the form of Research Fellowship in Science for Meritorious Students by University Grant Commission, Govt. of India, is gratefully acknowledged by one of the author B. Sharma. Authors also thank the members of MNCF, Indian Institute of Science, Bangalore, India for SEM and EDS measurements whereas SSCU unit of same institute is greatly acknowledged for XRD analysis.

### References

- [1]. T. W. Hickmott, Low-frequency negative resistance in thin anodic oxide films, *Journal of Applied Physics*, 33(9), 1962, 2669–2682.
- [2]. D. P. Matthew, B. S. Dmitri, L. B. Julien, J. J. Yang, S. Snider Gregory, R. S. Duncan, and R. Stanley Williams, Switching dynamics in titanium dioxide memristive devices, *Journal of Applied Physics*, 106, 2009, 074508 (1-6).
- [3]. S. Kim and Y-K Choi, Resistive switching of aluminum oxide for flexible memory, *Applied Physics Letter*, 92, 2008, 223508 (1-3).
- [4]. K-D Liang, C-H Huang, C-C Lai, J-S Huang, H-W Tsai, Y-C Wang, Y-C Shih, M-T Chang, S-C Lo, and Y-L Chueh, Single CuO<sub>x</sub> nanowire memristor: forming-free resistive switching behavior, *ACS Applied Materials & Interfaces*, 6(19), 2014, 16537-16544.
- [5]. C. Yu and H. Wang, Light-induced bipolar-resistance effect based on metal-oxide-semiconductor structures of Ti/SiO<sub>2</sub>/Si, *Advanced Material*, 22, 2010, 966–970.
- [6]. H. Wang, C. Zou, L. Zhou, C. Tian and D. Fu, Resistive switching characteristics of thin NiO film based flexible nonvolatile memory devices, *Microelectronic Engineering*, 91, 2012, 144–146.
- [7]. A. Sawa, T. Fujii, M. Kawasaki and Y Tokura, Hysteretic current-voltage characteristics and resistance switching at a rectifying Ti/Pr<sub>0.7</sub>Ca<sub>0.3</sub>MnO<sub>3</sub> interface, *Applied Physics Letters*, 85 (18), 2004, 4073–4075.
- [8]. X. Zhu, F. Zhuge, M. Li, K. Yin, Y. Liu, Z. Zuo, B. Chen and R-W Li, Microstructure dependence of leakage and resistive switching behaviours in Ce-doped BiFeO<sub>3</sub> thin films, *Journal of Physics D: Applied Physics*, 44, 2011, 415104 (7pp).
- [9]. J. Qi, M. Olmedo, J. Ren, N. Zhan, J. Zhao, J-G Zheng, and J. Liu, Resistive switching in single epitaxial ZnO nanoislands, *ACS Nano*, 6 (2 ), 2012, 1051-1058.
- [10]. Ouyang, Application of nanomaterials in two-terminal resistive-switching memory devices, *Nano Reviews*, 1, 2010, 5118.
- [11]. L. Y. Tao, L. S. Bing, L. Qi, L. H. Bing, L. Su and L. Ming, An overview of resistive random access memory devices, *Chinese Science Bulletin*, 56, 2011, 28-29.
- [12]. X. Qian, H. Liu, N. Chen, H. Zhou, L. Sun, Y. Li, and Y. Li, Architecture of CuS/PbS heterojunction semiconductor nanowire arrays for electrical switches and diodes, *Inorganic Chemistry*, (51), 2012, 6771–6775.
- [13]. V. Kannan and J. K. Rhee, Robust switching characteristics of CdSe/ZnS quantum dot non-volatile memory devices, *Physical Chemistry Chemical Physics*, 15, 2013, 12762-12766.
- [14]. D. Wu, Y. Jiang, Y. Yu, Y. Zhang, G. Li, Z. Zhu, C. Wu, L. Wang, L. Luo and J. Jie, Nonvolatile multibit Schottky memory based on single n-type Ga doped CdSe nanowires, *Nanotechnology*, 23, 2012, 485203 (7pp).
- [15]. J. Park, S. Lee, and K. Yong, Photo-stimulated resistive switching of ZnO nanorods, *Nanotechnology*, (23), 2012, 385707 (6pp).
- [16]. A. Younis, D. Chu, I. Mihail, and S. Li, Interface-engineered resistive switching: CeO<sub>2</sub> nanocubes as high performance memory cells, *ACS Applied Materials Interfaces*, 5, 2013, 9429–9434.
- [17]. J. H. Yoon, J. H. Han, J. S. Jung, W. Jeon, G. H. Kim, S. J. Song, J. Y. Seok, K. J. Yoon, M. H. Lee, and C. S. Hwang, Highly improved uniformity in the resistive switching parameters of TiO<sub>2</sub> Thin films by inserting Ru nanodots, *Adv. Mater.* 25, 2013, 1987–1992.
- [18]. M. J. Yun, H-D Kim, S. M. Hong, J. H. Park, D. S. Jeon, and T. G. Kim, Effect of embedded metal nanocrystals on the resistive switching characteristics in NiN-based resistive random access memory cells, *Journal of Applied Physics*, 115, 2014, 094305 (1-5).
- [19]. J-Y Lin and B-X Wang, Resistive switching effects of nanocrystalline silicon films in conductive-bridging random-access memory device, *Indian Journal of Engineering & Materials Sciences*, 20, 2013, 209-212.
- [20]. F-C Chiu, Conduction mechanisms in resistance switching memory devices using transport boron doped zinc oxide films, *Materials*, 7, 2014, 7339-7348.
- [21]. M. A. M. Khan, S. Kumar, M. Ahamed, S. A. Alrokayn and M. S. AlSalhi, Structural and thermal studies of silver nanoparticles and electrical transport study of their thin films, *Nanoscale Research Letter*, 6 (2011) 434 (1-8).
- [22]. W Sally, D. Solomon, M. Bahadory, A. V. Jeyarajasingam, S. A. Rutkowsky, and C. Boritz, Synthesis and study of silver nanoparticles, *Journal of Chemical Education*, 84 (2), 2007, 322-325.
- [23]. S. Agnihotri, S. Mukherji and S. Mukherji, Size-controlled silver nanoparticles synthesized over the range 5–100 nm using the same protocol and their antibacterial efficacy, *RSC Advances*, 4, (2014) 3974-3983.